Fluid Motion Generated by Impact

J. J. Monaghan[1]; A. Kos[2]; and N. Issa[3]

Abstract: In this paper we describe laboratory experiments and numerical simulations of the impact between a rigid body and water. The rigid body consists of a weighted rectangular box that slides down a curved ramp to enter the water at an angle to the horizontal of approximately 15°. As the box enters the water, a vigorous spray projects fluid beyond the box, then, as the water is heaved up, it falls back on the upper surface of the box and initiates a solitary wave. The experiments cover a wide range of impact velocities and three water depths in the main body of the tank. The experiments have been simulated using the Lagrangian particle method smoothed particle hydrodynamics (SPH).

DOI: 10.1061/(ASCE)0733-950X(2003)129:6(250)

CE Database subject headings: Rigid-body dynamics; Water flow; Impact; Lagrangian functions.

Introduction

The present work was motivated by consideration of block avalanches where a block of rock breaks loose, then runs down a slope into a body of water. However, the general question of the fluid motion produced by a solid body entering a fluid is of importance in other areas, principally in ship building and the design of off-shore rigs. In ships the pressure generated by impact can deform the bow area (Yamamoto et al. 1985), while for rigs it can be a significant source of fatigue.

Even for the simple two-dimensional problem of a wedge or cylinder entering an infinite body of water, with the motion of the wedge or cylinder specified and gravity neglected, exact analytical solutions do not exist (Korobkin 1988). Approximate solutions are available [see, for example, Mackie (1968) for the slender wedge, and for other early references concerning wedge impact, see Greenhow (1987)], but they are limited to the early stage of the impact. Numerical techniques based on the boundary element method of Vinje and Brevig (1981) give reasonable agreement with experiments for the initial stage of wedge entry, but for some wedge vertex angles the method fails (Greenhow 1987). Korobkin and Wu (2000) describe boundary and finite-element methods for the entry of a circular cylinder with a specified motion, but these methods have difficulties simulating the jet that forms shortly after entry, and they are incapable of describing the more complex flows we consider here.

For the present problem, a solid body moves down a ramp under gravity and enters the water down a beach. When the solid body enters the water, it does so by first pushing into a narrow wedge of water. It then slows down as a vigorous jet of water is projected from the front face. There are no useful analytical approximations for this problem, which requires the self-consistent solution of the body and the fluid motion in a fluid of changing depth. A related problem, where a solid wedge *initially under* the water surface slides down a slope, has been simulated using a volume of fluid technique (Assier Rzadkiewicz et al. 1997; Watts 2000), but the present problem is considerably more difficult, because a key feature is the entry into the fluid.

In this paper we investigate the impact of a solid body entering water using both laboratory experiments and numerical simulation. The experiments are for a wide range of entry velocities and three tank depths. The simulations use the Lagrangian particle method smoothed particle hydrodynamics (SPH) (e.g., Monaghan and Kos 1999), which has already been applied to a vertical impact (Monaghan and Kos 2000). There is good agreement between the simulations and the experiments.

Experiments

The experimental setup is illustrated in Fig. 1. This figure is not to scale but serves to show the main features of the experimental setup. The use of a curved ramp permits us to reduce the horizontal extent of the ramp while allowing the entry velocity to be varied over a wide range by changing the height from which the box is released. The height of the ramp measured from zero at the bottom of the ramp rises to 98.4 cm. The horizontal length of the ramp is 3.178 m. The ramp was constructed by building two straight sections with different slopes, then bending the plastic to fit between them. The height of the ramp y varies with the horizontal distance x measured from the bottom of the ramp according to the following. For $0 \leqslant x \leqslant 2$, $y = 0.178x$; for $2 < x \leqslant 2.978$, $y = 0.120 + 0.407x - 0.32x^2 + 0.0877x^3$; and for $2.978 < x \leqslant 3.178$, $y = -1.667 + 0.832x$, where all distances are in meters and values of y and its gradient at the fitting points are calculated to three significant figures. The ramp has a central raised guide that fits into guide rails fixed to the bottom of the box as shown in the inset in Fig. 1. This prevents the box moving sideways.

The details of the box are shown in the figure, where all measurements are in mm. The box rests on four teflon feet approximately 2 mm thick and 50 mm in diameter. The height of the box is 10.7 cm, its length is 30 cm, and its width is 38.5 cm. The

[1]Professor, School of Mathematical Sciences, Monash Univ., Clayton, Vic. 3800, Australia.

[2]School of Mathematical Sciences, Monash, Univ., Clayton, Vic. 3800, Australia.

[3]School of Mathematical Sciences, Monash Univ., Clayton, Vic. 3800, Australia.

Note. Discussion open until April 1, 2004. Separate discussions must be submitted for individual papers. To extend the closing date by one month, a written request must be filed with the ASCE Managing Editor. The manuscript for this paper was submitted for review and possible publication on July 3, 2001; approved on May 6, 2003. This paper is part of the ***Journal of Waterway, Port, Coastal, and Ocean Engineering***, Vol. 129, No. 6, November 1, 2003. ©ASCE, ISSN 0733-950X/2003/6-250–259/$18.00.

J. Waterway, Port, Coastal, Ocean Eng. 2003.129:250-259.

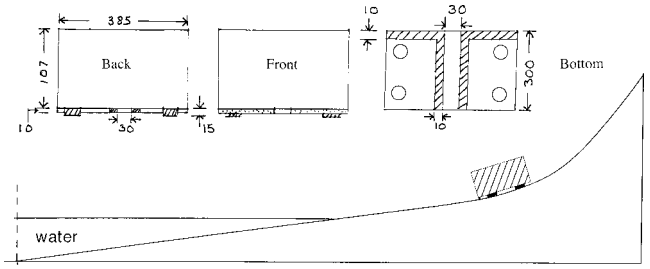

Fig. 1. Experimental setup (drawing not to scale)

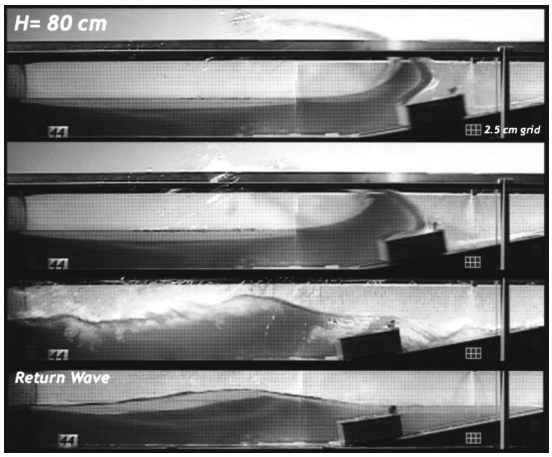

Fig. 2. Time sequence, starting at the top, taken from a video of the box entering the water at 2.3 m/s speed into water with a maximum depth of 21 cm. The last frame shows the returning wave. Note the heaving up of the water onto the box and the vigorous jet in frames 1 and 2, the disorder associated with the jet hitting the water, and the disorder in the flow in frame 3 caused partly by the catch at the back edge of the box. Frame 4 shows the return wave.

width of the box is slightly less than the width of the tank. For the experiments described here, the box was filled with granular material so that its total mass was 37.7 kg, giving it an average density of 3,050 kg/m^3. The dimensions of the tank are: length ~7 m, width 40 cm, and height 40 cm. A small shield (shown in Fig. 1) was placed at the bottom of the front of the box to reduce the flow of water under the box.

The coefficient of sliding friction between the box feet and the ramp proves to be an important quantity for the comparison between experiment and simulations. For the case of the dry ramp, it was determined by allowing the box to slide down the dry ramp, recording the position and time. The results were then compared with a numerical simulation and the best coefficient of friction was found. With a value for this coefficient of 0.1776, the difference between the simulation and the experiment was approximately 2%. In the experiments involving the entry of the box into the water, the friction effects are more complicated and will be discussed later.

In the experiments the weighted box was released from a range of heights and its motion was recorded on video tape. All measurements were made from the video frames and the timing of the frames, which were 0.04 s apart. Because the height of the dominant wave was determined relative to the 2.0 cm square grids in the background, and because its surface was distorted by small scale motion, the error in the wave height is ± 0.5 cm.

A typical sequence is shown in the four frames of Fig. 2, which are for water depth $D=21$ cm with entry speed V_0 of 2.3 m/s. In frame 1 the box is shown after it has entered the water and produced a vigorous jet of water that rises above the tank. The maximum height of the jet above the ambient water surface is given approximately by $0.6V_0^2/g$. At the base of the jet, a large body of water has been heaved up by the moving box and is settling to the top of the box. This water moves with the box for some time. In frame 2 the water that was heaved up is just in contact with the box, and the water from the jet is about to hit the placid water in front of the box. In frame 3 the water from the jet has hit the surface of the water and significantly disturbed it. The fluid heaved up and onto the box has initiated a large wave which, at the time of frame 3, has a peak at about two box lengths in front of the box and is moving to the left. Some of the water has flooded over the top of the moving box and is forming a small region of highly disordered fluid behind it. The motion behind the box is only very crudely two-dimensional, because the back of the top of the box has a raised catch that initially holds the box in position on the ramp. This catch strongly perturbs the flow over the rear of the box.

The large wave travels down the tank and reflects off the rear wall. In frame 4 of Fig. 2 the reflected wave, which is moving to the right, is shown. This wave is approximately the classical Kortweg de Vries solitary wave with height η (above the ambient water level) as a function of horizontal distance x (measured from its peak):

$$\eta = \frac{A}{\cosh^2(x/B)} \tag{1}$$

where $B=\sqrt{4D^3/(3A)}$. During the travel time, the small scale disorder caused by the jet has largely dissipated. In addition, while the wave travels down the tank, water flows over the box to approximately restore the original water level. The wave motion is very close to two-dimensional.

Similar results were obtained for all other speeds and depths. At the lowest entry speeds we considered, most of the water heaved up remained in front of the box, whereas for the highest speed entries, the water heaved up completely covered the top of the box, and some spilled over the rear. In all cases the water heaved up moved with the box momentarily then left the box to form the primary wave. Eventually, for high enough entry speeds, the fluid piled up will flow over the rear of box so rapidly that the formation of the wave will be impeded. This suggests that the amplitude of the return wave will eventually reach a limit. In a related context we note that, in the case of steady flow over a fixed box placed on the bottom of a constant level tank, the shallow water equations show that water level above the box tends to a fixed height as the speed of the flow increases.

In Fig. 3 we show the amplitude of the wave reflected from the end wall of the tank for various depths and speeds of entry. This amplitude is the maximum height of the wave above the ambient level of the water in the tank and it was measured approximately halfway between the left-hand end of the tank and the final position of the box. The measurements were taken from photographs. At the time when the amplitude was measured, we established that the ambient level was within 0.5 cm of its original level and that the amplitude remained constant until its peak was within 0.75 m of the final position of the box. The results show that for constant entry speeds the waves are greater when the tank depth is lower and dA/dV_0 decreases as V_0 increases.

J. Waterway, Port, Coastal, Ocean Eng. 2003.129:250-259.

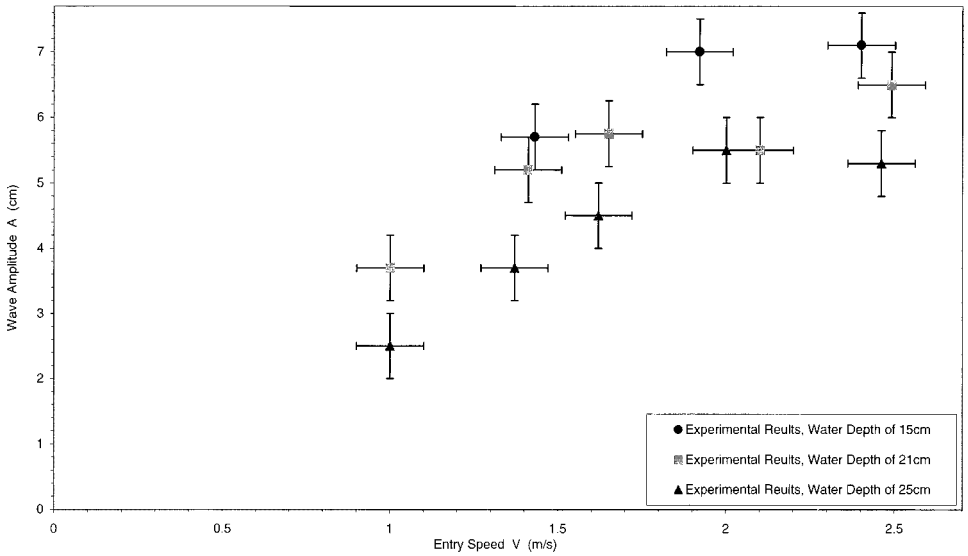

Fig. 3. Amplitude A of return wave as a function of box entry speed V_0 for three wave tank depths of 15, 21, and 25 cm

We can expect the amplitude A of the wave reflected from the end of the tank to be given by a general expression of the form

$$\frac{A}{D}=\Phi\left(\frac{V_0^2}{gH},\frac{H}{L},\frac{H}{D}\right) \tag{2}$$

where H=height of the box; L=its length; and Φ=arbitrary function. The experiments show that, for the range of V_0 we consider only a small fraction of the water heaved onto the box spills over its rear. Therefore, even if the box were longer, most of the motion would not be changed significantly. On the other hand, if L were much smaller, most of the water heaved up would flow over the back of the box, changing the wave initiation completely.

For the present experiments, L and H are fixed and we seek a relation of the form

$$\frac{A}{D}=\Phi\left(\frac{V_0^2}{gH},\frac{H}{D}\right) \tag{3}$$

The results shown in Fig. 3 suggest that we graph A/D against

$$V^*=\frac{V_0}{\sqrt{gH}}\left(\frac{H}{D}\right)^3 \tag{4}$$

The results are shown in Fig. 4. It can be seen from this figure that the results collapse onto a single curve. The solid line in Fig. 4 is given by

$$\frac{A}{D}=0.5\left[\frac{V_0}{\sqrt{gH}}\left(\frac{H}{D}\right)^3\right]^{1/2} \tag{5}$$

There is no simple model that produces this power law. For example, assuming the energy of the solitary wave is proportional to the energy of the box when it enters the water, and keeping the dominant terms, gives the relation

$$\frac{4}{3}g\rho_0 A^2 B\propto\frac{1}{2}MV^2 \tag{6}$$

and, using the definition of B after Eq. (1), we find

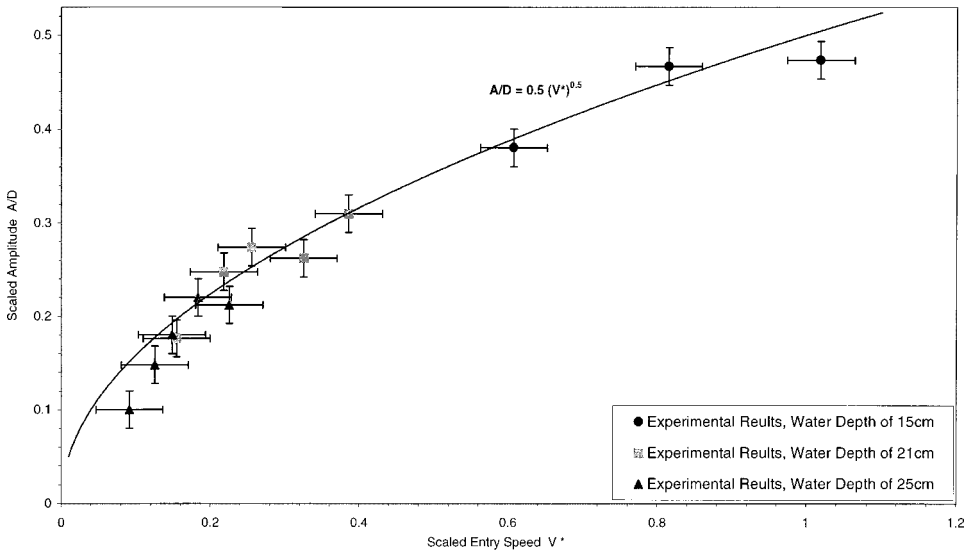

Fig. 4. Scaled experimental amplitude A^* against scaled entry speed V^*, defined in text; solid line is formula described in text

J. Waterway, Port, Coastal, Ocean Eng. 2003.129:250-259.

$$\frac{A}{D} \propto \frac{V^{4/3}}{D^2}$$

which gives an incorrect dependence on D and the entry speed of the box.

Although the agreement between this scaling relation and the experiments is satisfactory, there are limits to its applicability. We have already mentioned that the length of the box L plays a part in the formation of the wave which would be different for a much smaller L. In addition it is clear that, if H were so large that the water could not fall back onto the box, the results would be different.

Numerical Technique

Smoothed Particle Hydrodynamics Equations

The numerical method we use is smoothed particle hydrodynamics (SPH). For the earliest reference, see Gingold and Monaghan (1977), and for a review of this method in connection with astrophysical gas dynamics, see Monaghan (1992). For the early applications to nearly incompressible fluids, see Monaghan (1994). A recent application to waves on a beach with cliffs describes the details of the method (Monaghan and Kos 1999), and a study of a box falling vertically into a tank (Monaghan and Kos 2000) shows that the method gives good results for an impact problem. Other methods, such as the Constrained Interpolation Profile (CIP) method of Yabe [Wang et al. (1993) and for a review see Yabe et al. (2001)], could be applied to this problem, but we do not expect CIP to treat the splash as simply as SPH, although it is capable of giving very good results for the bulk features of the flow. The Moving Particle Semi-Implicit (MPS) method due to Koshizuka et al. (1998) uses particles and kernels, as in the SPH method, but calculates the pressure and density in a different way. Because the kernels used by Koshizuka et al. (1998) do not have continuous first derivatives, the fluctuations can be expected to be larger than with SPH for the same number of particles. Furthermore, the gradient of the pressure is constructed in such a way that momentum is not conserved exactly. For these reasons we prefer the SPH method.

The key feature of the SPH method is the use of moving interpolation points that can be thought of as particles. Each particle carries a fixed mass and has velocity v which is representative of the fluid in its neighborhood. The equations are derived from the Navier Stokes equations using a kernel interpolation technique which transforms the partial differential equations into ordinary differential equations for the properties of each particle. The basic ideas of SPH are described in detail in Monaghan (1992), and its application to almost incompressible fluids is described by Monaghan and Kos (1999). We therefore confine our description to the principal issues.

The acceleration equation for the fluid

$$\frac{dv}{dt} = -\frac{1}{\rho}\nabla P + \frac{\mu}{\rho}\nabla^2 v + g \tag{7}$$

where P=pressure; ρ=density; μ=coefficient of viscosity; and g=gravitational acceleration. In addition, although it is not made explicit, there are surface forces due to the moving rigid body. The SPH form of Eq. (7) for particle a is

$$\frac{dv_a}{dt} = \sum_b m_b \left(\frac{P_a}{\rho_a^2} + \frac{P_b}{\rho_b^2} + \Pi_{ab} \right) \nabla_a W_{ab} + \sum_k f_{ak} + g \tag{8}$$

The first summation is over neighboring fluid particles and represents the pressure and viscous terms. The second summation is over the boundary particles. Boundary particle k exerts a force f_{ak} per unit mass on the fluid particle a. These boundary particles may represent fixed or moving boundaries. The mass of particle b is m_b and the interpolating kernel is W_{ab}, which is a function of $r_{ab}=|r_a-r_b|$. The gradient of the kernel with respect to the coordinates of particle a is denoted by $\nabla_a W_{ab}$. The length scale of the kernel (see the following) is denoted by h. The function Π_{ab} provides the viscosity [for details, see Monaghan (1992) and Monaghan and Kos (1999)]. In this paper, W is the cubic spline kernel normalized for two dimensions (Monaghan 1992).

The pressure is calculated from an equation of state

$$P = E\left[\left(\frac{\rho}{\rho_0} \right)^{\gamma} - 1 \right] \tag{9}$$

where the parameter E is chosen so that the speed of sound is sufficiently large to ensure the Mach number is $\leqslant 0.1$, and we note that the density fluctuations $\delta\rho/\rho$ are then ~ 0.01, so that the fluid is nearly incompressible. In the present case we choose $E = 100\rho_0 V_0^2/\gamma$ and the speed of sound $c_s = 10V_0$. The constant $\gamma \sim 7$ determines the stiffness of the material, though the calculations are not sensitive to γ, because the density variations are so small the equation of state can be linearized. Numerous tests (Monaghan and Kos 1999, 2000; Monaghan et al. 1999) show that this choice of E gives very satisfactory results.

The disadvantage of using an equation of state with a low Mach number is that the time steps are shorter than if an implicit technique is used (in the present case, by a factor of 10). However, most implicit techniques require iteration so that the loss of efficiency is not excessive. The advantage of this is that the explicit integration leads to very simple codes.

Motion of Rigid Body

The motion of the rigid body is determined by specifying the motion of the center of mass and the rotation about the center of mass. We assume the motion is in two dimensions. The equation of motion of the center of mass R of a rigid body of mass M is given by

$$M\frac{dV}{dt} = F \tag{10}$$

where V=velocity of the center of mass; and F=total force on the body. The equation for the angular velocity Ω about the center of mass is

$$I\frac{d\Omega}{dt} = \tau \tag{11}$$

where I=moment of inertia (a scalar for the present case); and τ=total torque about the center of mass.

The rigid body is represented in the computation by a set of boundary particles that are equi-spaced around the boundary. These particles interact with the fluid particles. On a macro scale, they mimic the boundary atoms of the actual rigid body. The technique of replacing moving boundaries by particles is due to Peskin (1977).

Denoting the force per unit mass on rigid body boundary particle k by f_k, the previous equations become

$$M\frac{dV}{dt} = \sum_k m_k f_k \tag{12}$$

J. Waterway, Port, Coastal, Ocean Eng. 2003.129:250-259.

and

$$I\frac{d\Omega}{dt}=\sum_k m_k(r_k-R)\times f_k \tag{13}$$

where the direction of Ω is perpendicular to the plane of the motion. The rigid body boundary particles move as part of the rigid body, so that the change in position of boundary particle k is given by

$$\frac{dr_k}{dt}=V+\Omega\times(r_k-R) \tag{14}$$

The force per unit mass f_k on the boundary particle k is due to the fluid particles unless the moving rigid body strikes a fixed boundary. Neglecting this latter case we can write

$$f_k=\sum_a f_{ka} \tag{15}$$

where f_{ka} denotes the force per unit mass on boundary particle k due to fluid particle a and the summation is over the fluid particles. The precise form of this force depends on how the boundary force is implemented. However, to ensure that linear and angular momentum of the entire system is conserved in the absence of external forces, the force on a due to k must be equal and opposite to the force on k due to a. If the perpendicular distance from the boundary particle to the fluid particle is denoted by y and the tangential distance by x, then a suitable form is

$$f_{ka}=-\frac{m_a}{m_a+m_k}B(x,y)n_k \tag{16}$$

and n_k=unit normal at the position of boundary particle k directed from the boundary to the fluid. Similarly the force per unit mass on fluid particle a due to boundary particle k is

$$f_{ak}=\frac{m_k}{m_a+m_k}B(x,y)n_k \tag{17}$$

so that the forces $m_k f_{ka}=-m_a f_{ak}$ are equal and opposite.

In the absence of external forces, and recalling that the gradient of the kernel has odd symmetry with respect to its argument, we can deduce from Eq. (8) that

$$\sum_a m_a\frac{dv_a}{dt}=\sum_a\sum_k m_a f_{ak} \tag{18}$$

The right-hand side can be written

$$-\sum_k m_k f_k=-M\frac{dV}{dt} \tag{19}$$

which shows that total linear momentum

$$\sum_a m_a v_a+MV$$

is conserved. Total angular momentum is also conserved, though we do not give the proof here. These results assume a rigid body interacting with a fluid without fixed boundaries and external forces.

When the rigid body can interact with a fixed boundary, the fixed and moving boundary particles interact with the force specified by Eq. (21), with n chosen along the line of centers of the interacting particles. Of course once the fluid or the rigid body interacts with fixed walls, or are subject to external forces, momentum is not conserved.

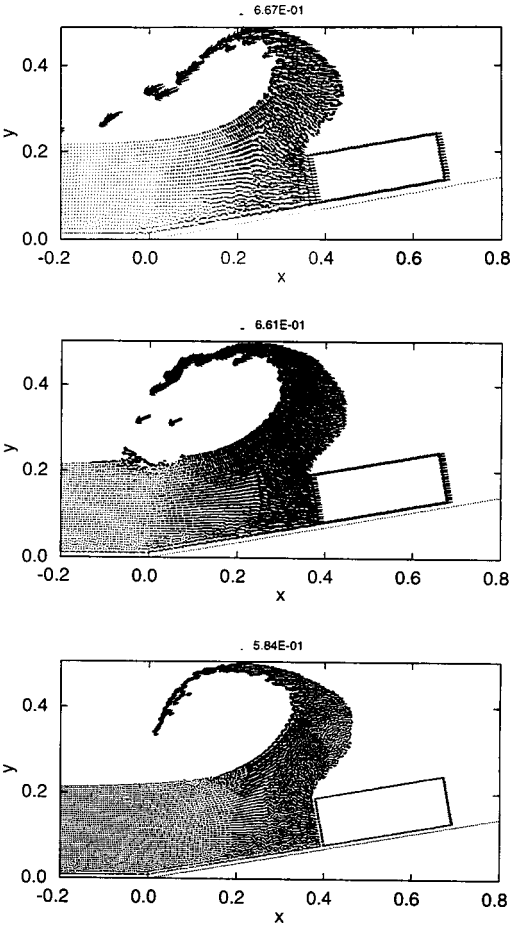

Fig. 5. Three frames shown are for the SPH simulation of the entry of a box into water for three resolutions, $D/30$, $D/40$, and $D/50$, with coarsest resolution at the top. Other details are given in the text. Note the resolution dependence of the jet and the insensitivity to resolution of the main features of the flow.

Boundary Forces

The previous sections have defined boundary forces in terms of a function $B(x,y)$ where $x\geq 0$ and $y\geq 0$ are local cartesian coordinates measured tangential and perpendicular to the boundary, respectively. In particular, y equals $n_k\cdot r_{ak}$. We write $B(x,y)$ as a product $\Gamma(y)\chi(x)$, where the function $\chi(x)$ is defined by

$$\chi(x)=\begin{cases}\left(1-\dfrac{x}{\Delta p}\right) & \text{if } 0<x<\Delta p\\ 0 & \text{otherwise}\end{cases}$$

where Δp=boundary particle spacing. The function $\Gamma(y)$ is defined in terms of the variable $q=y/h$ and a function that has the form of the gradient of the kernel. This function has a maximum at $q=2/3$. For $0<q<2/3$, we replace the value of the function by its maximum. Accordingly

$$\Gamma(y)=\begin{cases}\dfrac{2}{3}\beta & \text{if } 0<q<2/3\\ \beta\left(2q-\dfrac{3}{2}q^2\right) & \text{if } 2/3<q<1\\ \dfrac{1}{2}\beta(2-q)^2 & \text{if } 1<q<2\\ 0 & \text{otherwise}\end{cases}$$

J. Waterway, Port, Coastal, Ocean Eng. 2003.129:250-259.

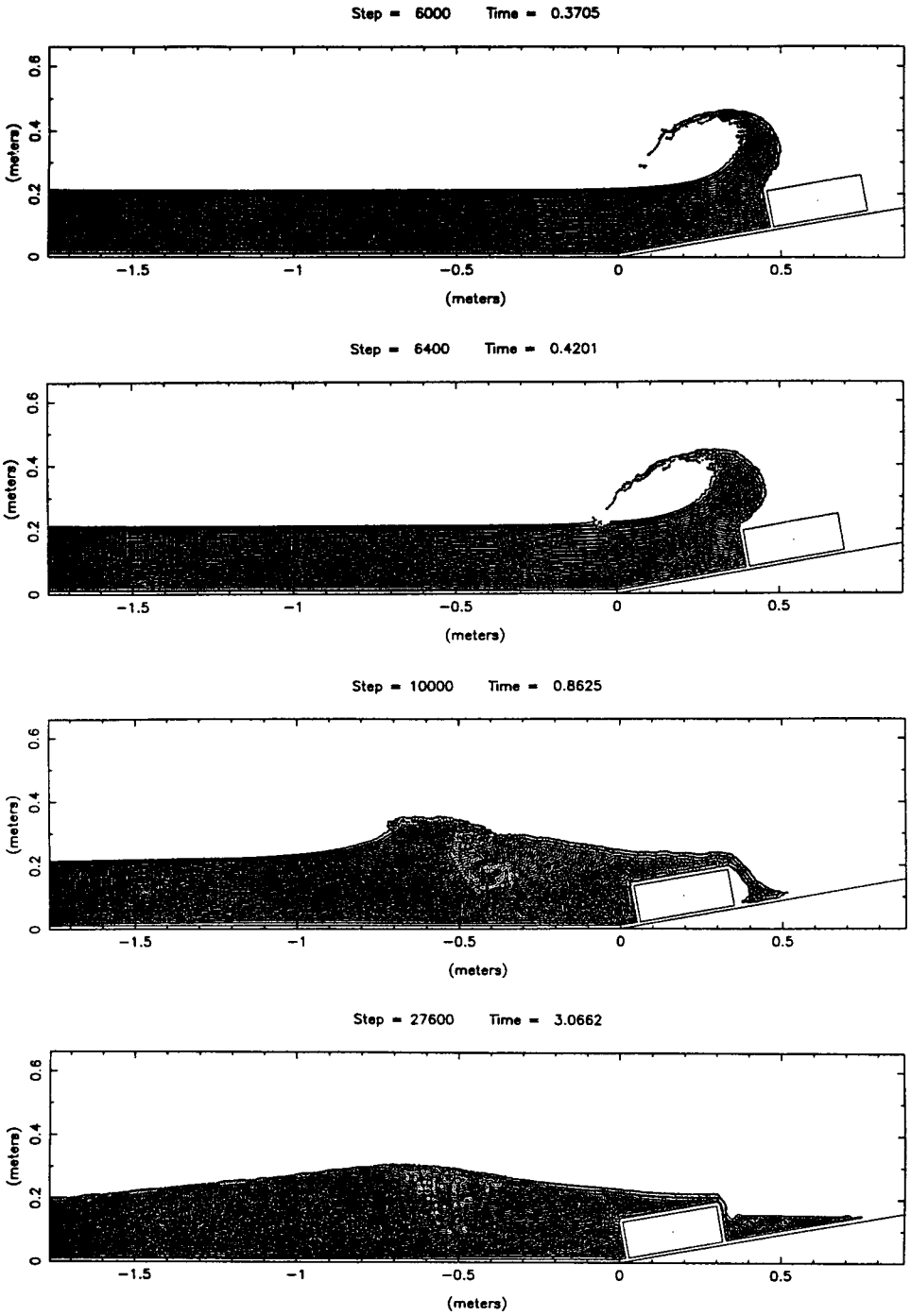

Fig. 6. Time sequence of SPH particles for simulation with same entry speed and water depth as in Fig. 2

where β is $0.02c_s^2/y$. This term is an estimate of the maximum force/mass necessary to stop a particle moving at the estimated maximum speed. The factor $1/y$ ensures that a faster moving particle can be stopped. In a previous simulation (Monaghan and Kos 1999), we used a different form of the boundary force. The present form was chosen because the boundary force opposes the pressure gradient and this is constructed by using a gradient of a kernel. However, in practice, the new choice of boundary force makes only slight differences to the final results. The optimum boundary force is not known.

For simulations where a corner of the rigid body can hit the bottom of the tank, we need to take account of the fact that it must be stopped, though only a few of the particles near the corner are interacting with the bottom of the tank. The factor $1/y$ can, in principle, take care of the problem, but in the simulations we multiply β by the factor $(1+M^*)$ where M^* is the ratio of the mass of the rigid body to the mass of an equal volume of water.

The rigid body and the tank have corners. We treat the corner particles differently from the other boundary particles. They may interact with a fluid particle using one or another of the normals to the lines that make up the corner, or along the line joining the boundary and fluid particles in such a way that there is a smooth transition for a flow around a corner. The first task is to allow the corner particles to be recognized easily in the program. This is done by assigning a normal to the jth corner particle with the x component $n_x=1+j$. This immediately identifies the particle as a

J. Waterway, Port, Coastal, Ocean Eng. 2003.129:250-259.

corner particle (all other particles have $n_x \leqslant 1$) and identifies that it is the jth corner particle in a list of corner particles. The normals are found by looking up two lists. The jth entry on one list contains the label of the boundary particle on one side of particle j, and the jth entry of the other list contains the label of the particle on the other side. These are not corner particles, and they have the usual unit normals. Denote these normals by n_1 and n_2 and let the vector from corner particle k to fluid particle a be r_{ak}. We then proceed as follows:

If the fluid particle lies between the wedge defined by n_1, n_2, and the corner particle, the quantity $S=(n_1\times r_{ak})\cdot(n_2\times r_{ak})$ will be negative. In this case the boundary force is used along the direction of r_{ak}, i.e., along the radial line connecting the two particles. If $S>0$ then the fluid particle is not in this wedge and one or another of the normals should be used. If $n_1\cdot r_{ak}>n_2\cdot r_{ak}$, the fluid particle is within the region formed by the extension of n_1 at the corner, and the side with this normal. Accordingly we use n_1 as the direction of the force from the corner particle to the fluid particle. If the inequality is reversed, we use n_2.

Modeling Friction

In addition to the forces already mentioned, there are frictional forces that must be included. The simplest of these is the friction between the feet of the box and the ramp. A more complicated form of friction is due to fluid motion between the box and the ramp and between the box and the walls.

In principle the friction force on the feet can be taken into account by determining the force on the box normal to the ramp F_n and including a force $\hat{\mu}_f F_n$ opposite to the tangential component of the velocity where $\hat{\mu}_f=0.1776$ is the coefficient of dynamic friction. As mentioned previously, this was determined by running the box down a dry ramp and comparing the results with a simulation.

In the first part of the motion, all four feet slide on the dry ramp. On entering the water the front two feet slide through the water. We performed experiments with the box sliding down a wet ramp and found that the coefficient of static friction was within a few percent of the coefficient for the dry ramp. However, static friction on a wet ramp is not necessarily a good indicator of the appropriate dynamic friction when the teflon feet enter the water. For this reason we have run simulations with no friction, the full dry sliding friction $\mu_f \sim 0.1776$, and a reduction of 0.5 in the friction for each set of feet entering the water. In this last case we use the average coefficient of friction. Thus, with two feet only in the water the coefficient of friction is $0.75\,\mu_f$, and with all four feet in the water the coefficient of friction is $0.50\,\mu_f$.

The hydrodynamic contribution to the friction is much more difficult to include. This friction is due to viscosity, and an estimate of the magnitude of this source of friction with reasonable accuracy would require a full three-dimensional calculation. In this paper we therefore limit ourselves to implementing the simple sliding friction model. In our simulations it appears that the full friction coefficient gives the best fit to the experimental results for a depth of 25 cm, while for the depth of 15 cm the average coefficient is best.

Time Stepping

We use a predictor-corrector leapfrog for time stepping, which we have found to be more accurate and just as stable as the improved Euler method used previously (Monaghan and Kos 1999). To integrate the set of equations describing the change of velocity v, density ρ, and position r given by

$$\frac{dv}{dt}=F \tag{20}$$

$$\frac{dr}{dt}=v \tag{21}$$

and

$$\frac{d\rho}{dt}=D \tag{22}$$

we denote the values of the variables at the beginning of a time step by v^0, F^0, r^0, ρ^0, D^0 and the time step by Δt. The predictor step is

$$v_p=v^0+\Delta t F^0 \tag{23}$$

$$r=r^0+\Delta t v^0+\frac{1}{2}(\Delta t)^2 F^0 \tag{24}$$

and

$$\rho_p=\rho^0+\Delta t D^0 \tag{25}$$

The value for r is not corrected. New values of F and D are calculated using the predicted quantities, and then corrected values of v and ρ are calculated according to

$$v=v_p+\frac{1}{2}\Delta t(F_p-F^0) \tag{26}$$

and

$$\rho=\rho_p+\frac{1}{2}\Delta t(D_p-D^0) \tag{27}$$

The time step is determined by the Courant condition and the boundary forces. The Courant condition is that $\delta t_c=0.5h/c_s$. The boundary force time step rule can be determined from the magnitude of the boundary force. We take $\delta t_w=\min_a y/(0.1c_s)$, where y is defined previously in connection with the boundary forces and the minimum is over all the particles. The time step used is then the minimum of the δt_c and δt_w. For typical simulations we use 15,000 particles and 20,000 time steps. This takes about 45 min on a Macintosh G4.

Numerical Simulations

Early tests of the SPH simulation technique (Monaghan 1994) showed that, even with rather crude resolution, it gave good results for dam collapse and bores. The simulation technique has been checked for wave propagation by comparison with other calculation techniques and by comparison with experiments (Monaghan and Kos 1999). Further tests involved the impact of a vertically moving weighted box (Monaghan and Kos 2000) and showed that the motion of the box and the wave motion were faithfully predicted by SPH. The motion of the box down the curved ramp without fluid interactions was checked and found to agree with the experiments to within a few percent. We assume the motion is two-dimensional and that the effects of the air can be neglected. Similarly we neglect the flow between the box and the side walls of the tank and the effects of the catch at the rear of the box. In order to reduce the computation time the model tank was 4.2 m long. While this is substantially shorter than the laboratory tank, which is ~7 m long, it is still much longer than the width of the reflected wave, which is typically ~1 m.

J. Waterway, Port, Coastal, Ocean Eng. 2003.129:250-259.

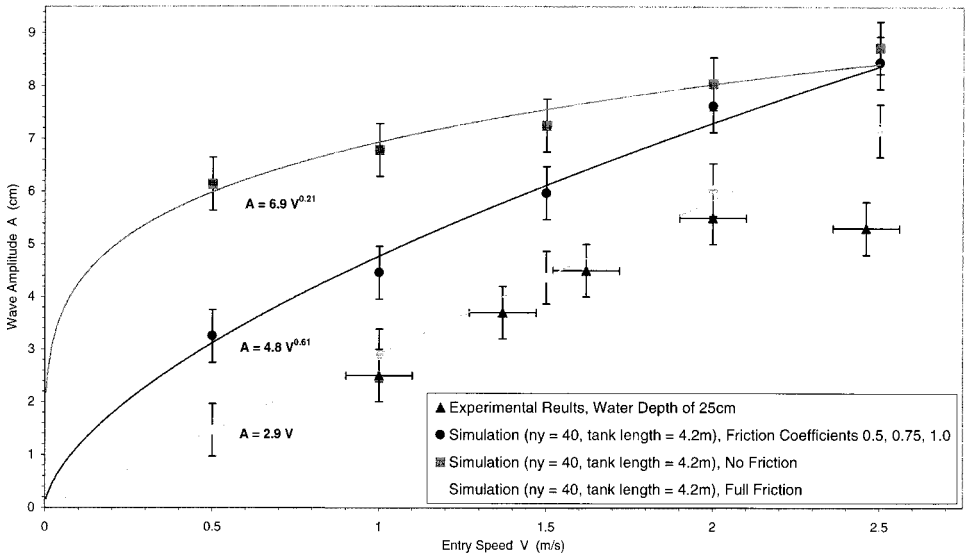

Fig. 7. Comparison between the amplitude of the primary solitary wave from the simulations and the experiments for 25 cm depth and different friction models. The upper continuous curve is for the simulation with no friction. The lowest continuous curve is for the simulation with constant friction. The intermediate curve is for the friction rule described in the text.

The convergence of the method has been discussed by Monaghan and Kos (2000). For the present problem we ran simulations with particle spacing equal to $D/30$, $D/40$, and $D/50$ for $D=21$ cm, at times of 0.494, 0.494, and 0.488, respectively. The SPH particles with attached velocity vectors are shown in Fig. 5. Though there are differences of detail, especially in form of the jet, the results for the different resolutions are very similar. The details of the jet depend on the resolution of the thin wedge of water the box first impacts. Since the particles in this simulation have the same mass and occupy the same volume, the resolution in this thin wedge is very poor, so the front of the jet varies noticeably as the resolution changes. The bulk of the jet, however, is well resolved with particle spacing $D/40$. These results concerning resolution are in agreement with those for a vertically falling box discussed by Monaghan and Kos (2000).

In Fig. 6 we show the appearance of the box and the fluid for the same initial conditions as for Fig. 2. The qualitative agreement with Fig. 2 is very good. The simulation reproduces the jet, the heaving of the water onto the box, and the flow over the rear of the box. However, it is clear that some details of the flow are not reproduced. As mentioned earlier, an accurate simulation of the jet requires a much greater resolution in the narrow wedge of fluid first met by the box. In addition, the air trapped under the water heaved onto the box and the catch at the rear of the box will introduce disorder into the flow that cannot be captured by our simplified two-dimensional calculation.

In Fig. 7 we compare the simulated and experimental primary wave for the case where $D=25$ cm for a range of V_0. The simulation results are shown by solid lines that denote different rules for the sliding friction. The best approximation to the experimen-

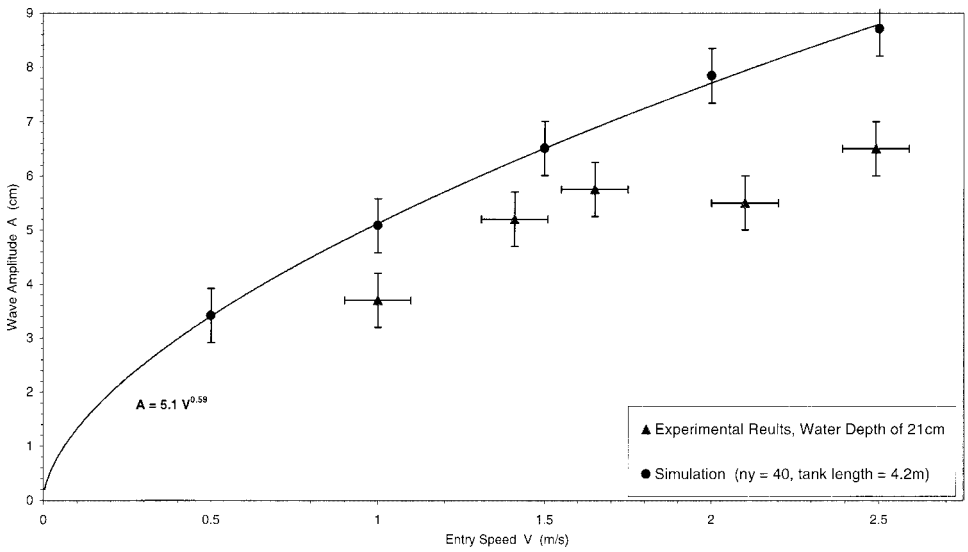

Fig. 8. Comparison between the experiments and the SPH simulation for a water depth of 21 cm. The simulation results use the reduced friction rule described in the text. The simulation results are shown by a continuous line.

J. Waterway, Port, Coastal, Ocean Eng. 2003.129:250-259.

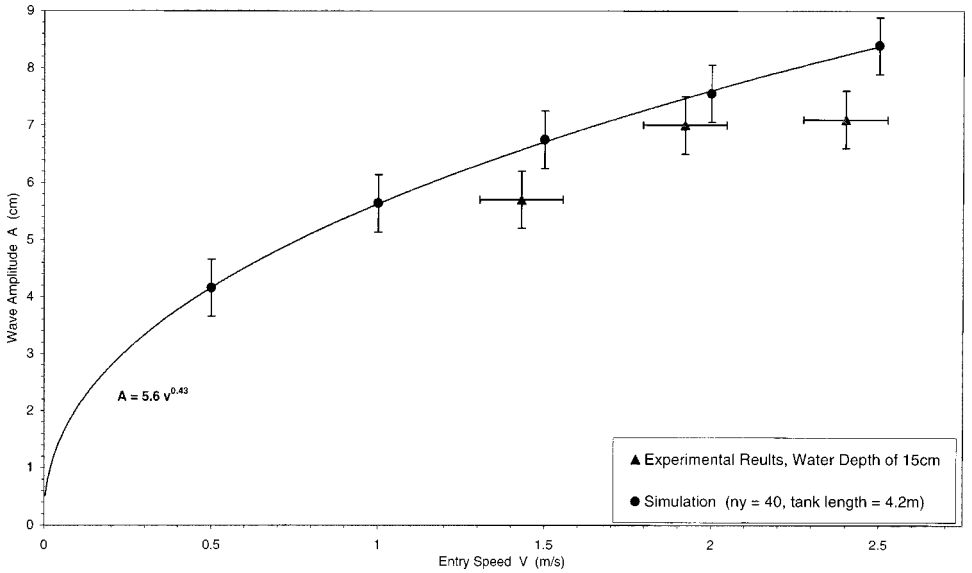

Fig. 9. Comparison between the experiments and the SPH simulation for a water depth of 15 cm. The simulation results use the reduced friction rule described in the text. The simulation results are shown by a continuous line.

tal wave amplitude for this case is obtained when the friction between the box and the ramp is the same as for a dry ramp. In this case, the experiments and simulations agree to within ~10% except for the highest entry speed. When the average friction law is used, the errors are typically ~50%.

In Figs. 8 and 9 we show the amplitude of the wave reflected from the end wall of the tank as a function of box speed for the experiments and the simulation depths of 21 and 15 cm. For the simulations the average friction law was used. The errors for the depth of 21 cm are ~20% except for the higher entry speeds, where the error is much larger. For the depth of 15 cm the errors are ~12%. These results indicate that no simple friction law is universally applicable for this problem. Fig. 10 shows the simulation results for all three depths scaled in the same way as in Fig. 4. These results indicate that a curve similar to that which fits the experimental results also gives a satisfactory fit to the SPH results.

In these simulations, errors occur because both continuum equations are approximated by SPH particles and because the friction law has been approximated. Numerous comparisons in other problems [Monaghan et al. (1999) for gravity currents, Monaghan and Kos (1999) for waves on a beach, and Monaghan and Kos (2000) for a falling box] show that, at the resolution used for the present problems, the errors arising from discretization are typically 5–10% of the magnitude, depending on the type of problem. The simulations just discussed indicate the sensitivity of the simulated reflected wave to the modeling of the friction law. With the best choice of the friction laws we have used, it is clear

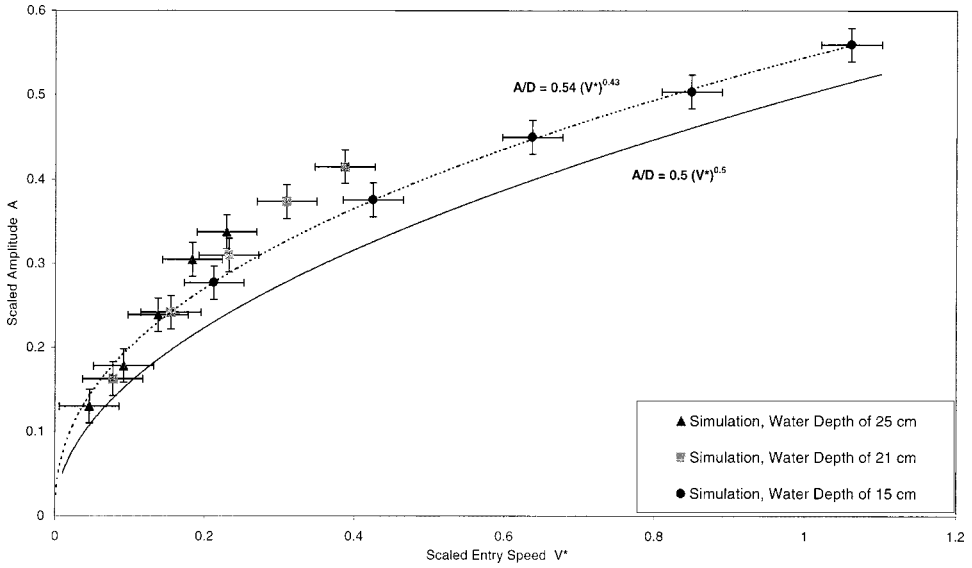

Fig. 10. Simulation results scaled in same way as experimental results shown in Fig. 4

J. Waterway, Port, Coastal, Ocean Eng. 2003.129:250-259.

that the friction law adds errors of several percent to the errors from using SPH.

Discussion and Conclusions

The results of this paper show that the essential features of the impact and entry of a rigid body (a box) traveling down a slope into water are: (1) the projection of a substantial jet of water into the air; (2) the heaving up of a mass of water; and (3) the formation of a solitary wave. The experiments not only establish the main features of the dynamics, but also allow us to estimate a scaling relation between the amplitude of the wave in terms of the properties of the rigid body at entry. As remarked earlier, the scaling relation for the wave amplitude is dependent on the geometry of the box. A very much shorter or much higher box would be expected to behave differently.

The SPH simulation technique reproduces the qualitative features of the entire process and gives satisfactory results for the wave amplitude, although they are dependent on the model chosen for the friction. This is a complicated problem, and a simulation of high accuracy would require other physical effects to be introduced. The first of these is the formation of bubbles by trapped air. To simulate the bubbles would require a major increase both in algorithm development and in the computational work. The second physical effect is associated with the flow in the narrow gaps under the box and between the box and the sidewalls of the tank. As remarked earlier, this flow can contribute to the effective friction, especially for large V_0, and may explain a significant part of the discrepancy between the amplitudes for the experiment and the simulation. However, a study of these effects would require a full three-dimensional simulation with very high resolution in the narrow gaps. As is often the case in numerical fluid dynamics, to get much better than 10% agreement with experiments requires an enormous amount of extra work.

Provided the errors in the simulations described here can be tolerated, the 2D SPH simulations can be easily extended to bodies with arbitrary shape and to cases where the slope and bottom of the tank have a more complicated geometry. These only require a different arrangement of the boundary particles.

Notation

The following symbols are used in this paper:

A = amplitude of the returning wave;
B = scale length in Kortweg de Vries formula for the amplitude;
D = depth of the water in the tank;
E = coefficient for the equation of state;
F = total force on the box;
g = gravitational acceleration;
H = height of the front of the box;
h = resolution length of the SPH kernel;
I = moment of inertia of the box;
L = length of the box;
M = total mass of the box;
m_b = mass of SPH particle b;
n = unit normal to the wall;
P_a = pressure at particle a;
R = center of mass of the box;
r_b = position of particle b;
r_{ab} = $r_a - r_b$;
V = velocity of the box;
V_0 = entry speed of box;
v_{ab} = $v_a - v_b$;
v_b = velocity of particle b;
$\hat{v}_b$ = smoothed velocity of particle b;
W_{ab} = $W(|r_a - r_b|)$ = SPH kernel;
γ = index for the artificial equation of state;
ρ_a = density at particle a;
μ = coefficient of viscosity;
μ_f = coefficient of sliding friction; and
Ω = angular velocity of the box.

References

Assier Rzadkiewicz, S., Mariotti, C., and Heinrich, P. (1997). "Numerical simulation of submarine landslides and their hydraulic effects." *J. Waterw., Port, Coastal, Ocean Eng.*, 123(4), 149–157.

Gingold, R. A., and Monaghan, J. J. (1977). "Smoothed particle hydrodynamics." *Mon. Not. R. Astron. Soc.*, 181, 375.

Greenhow, M. (1987). "Wedge entry into initially calm water." *Appl. Ocean. Res.*, 9, 214–223.

Korobkin, A. A. (1988). "Initial stage of water impact." *Annu. Rev. Fluid Mech.*, 20, 159–185.

Korobkin, A. A., and Wu, G. X. (2000). "Impact of a floating circular cylinder." *Proc. R. Soc.*, 456, 2489–2514.

Koshizuka, S., Nobe, A., and Oka, Y. (1998). "Numerical analysis of breaking waves using the moving particle semi-implicit method." *Int. J. Numer. Methods Fluids*, 26, 751.

Mackie, A. G. (1968). *Q. J. Appl. Mech.*, 22, 1.

Monaghan, J. J. (1992). "Smoothed particle hydrodynamics." *Ann. Rev. Astron. Ap.*, 30, 543–573.

Monaghan, J. J. (1994). "Simulating free surface flows with SPH." *J. Comput. Phys.*, 110, 399–406.

Monaghan, J. J., Cas, R. F., Kos, A., and Hallworth, M. (1999). "Gravity currents descending a ramp in a stratified tank." *J. Fluid Mech.*, 379, 36–39.

Monaghan, J. J., and Kos, A. (1999). "Solitary waves on a Cretan beach." *J. Waterw., Port, Coastal, Ocean Eng.*, 125(3), 145–154.

Monaghan, J. J., and Kos, A. (2000). "Scott Russell's wave generator." *Phys. Fluids A*, 12, 662–630.

Peskin, C. S. (1977). "Numerical analysis of blood flow in the heart." *J. Comput. Phys.*, 25, 220–252.

Vinje, T., and Brevig, P. (1981). "Numerical simulation of breaking waves." *Adv. Water Resour.*, 4, 77–82.

Watts, P. (2000). "Tsunami features of solid block underwater landslides." *J. Waterw., Port, Coastal, Ocean Eng.*, 126(3), 144–152.

Wang, P.-Y., Yabe, T., and Aoki, T. (1993). "A general hyperbolic solver—the CIP method applied to curvilinear coordinates." *Physical Soc. Japan*, 62, 1865–1871.

Yabe, T., Xiao, F., and Utsumi, T. (2001). "The constrained interpolation profile method for multi-phase analysis." *J. Comput. Phys.*, 169, 556–593.

Yamamoto, Y., Iida, K., Fukasawa, T., Murakami, T., Arai, M., and Ando, A. (1985). "Structural damage analysis of a fast ship due to bow flare slamming." *Int. Shipbuilding Prog*, 32, 124–136.

J. Waterway, Port, Coastal, Ocean Eng. 2003.129:250-259.